Short Communication

Sub-Volume Averaging of Repetitive Structural Features in Angularly Filtered Electron Tomographic Reconstructions

(electron tomography / missing wedge / limited specimen tilting / sub-volume averaging)

L. KOVÁČIK[1], S. KEREÏCHE[1], P. MATULA[2], I. RAŠKA[1]

[1]Institute of Cellular Biology and Pathology, First Faculty of Medicine, Charles University in Prague, Czech Republic
[2]Centre for Biomedical Image Analysis, Faculty of Informatics, Masaryk University, Brno, Czech Republic

Abstract. Electron tomographic reconstructions suffer from a number of artefacts arising from effects accompanying the processes of acquisition of a set of tilted projections of the specimen in a transmission electron microscope and from its subsequent computational handling. The most pronounced artefacts usually come from imprecise projection alignment, distortion of specimens during tomogram acquisition and from the presence of a region of missing data in the Fourier space, the "missing wedge". The ray artefacts caused by the presence of the missing wedge can be attenuated by the angular image filter, which attenuates the transition between the data and the missing wedge regions. In this work, we present an analysis of the influence of angular filtering on the resolution of averaged repetitive structural motives extracted from three-dimensional reconstructions of tomograms acquired in the single-axis tilting geometry.

Received June 27, 2014. Accepted July 21, 2014.

The work was supported by the grants: OPVK CZ.1.07/2.3.00/30.0030 from the Ministry of Education, Youth and Sports of the Czech Republic, P302/12/G157 and 13-32339P from the Czech Science Foundation, Prvouk/1LF/1 and UNCE204022 from Charles University in Prague, BIOCEV – Biotechnology and Biomedicine Centre of the Academy of Sciences and Charles University (project CZ.1.05/1.1.00/02.0109 of the European Regional Development Fund), and by grant No. CZ.2.16/3.1.00/24010 from the OPPK programme of the European Fund for Regional Development.

Corresponding author: Lubomír Kováčik, ICBP, First Faculty of Medicine, Charles University in Prague, Albertov 4, 128 01 Prague 2, Czech Republic. Phone: (+420) 224 968 000; Fax: (+420) 224 917 418; e-mail: lubomir.kovacik@lf1.cuni.cz

Abbreviations: 3D – three-dimensional, EM – electron microscopy, ET – electron tomography, FSC – Fourier shell correlation, NAD – non-linear anisotropic diffusion, PFR – para-flagellar rod, TEM – transmission electron microscopy.

Introduction

In electron tomography, three-dimensional reconstructions are computed from a set of tilted projections of a region of interest (a tomogram) acquired in a transmission electron microscope (TEM). Unfortunately, the computed three-dimensional (3D) reconstructions often suffer from severe artefacts that arise from an imprecise projection alignment, from the instability of specimen's structure during tomogram acquisition, and from the inability to record projections in the full tilting range of ± 90°. In a TEM, the range of angular tilting of the typical ~100-300 nm thick specimen slices is restricted not only due to the design of TEM's lenses, specimen holders and specimen supporting grids, but also by the increasing effective thickness of the inspected specimen slices at tilting (Koster and Barcena, 2006; Penczek and Frank, 2006). Since two-dimensional Fourier-transformed projections are central sections through 3D Fourier space of the object being reconstructed (Frank, 2006a), it is obvious that a portion of the 3D Fourier space does not contain any experimental data due to the limited tilting range. This portion of the Fourier space is usually referred to as the "missing wedge". At the single-axis tilting projection acquisition scheme, the missing wedge has a form of a sharply delimited double V-shaped region. Its Fourier transformation leads to the well-known impulse response (e.g., Komrska, 1983; Carazo, 1992; Kovacik et al., 2014), which gives rise to three typical artefacts: (1) four pairs of side rays of relatively low intensity but infinite in length, emanating from the neighbourhood of the central spot of the impulse response (Komrska, 1983), (2) elongation of the reconstructed features in the direction of the axis of the missing wedge, and (3) side minima joining the central spot in the direction of the x-axis.

In our previous paper (Kovacik et al., 2014) we have introduced an angular filter, which dampens the sharp transition of the data-covered portion of the Fourier space of the reconstructed object to the missing wedge area, so that it basically acts as a directional filter reducing both the length and the intensity in the ray artefacts

of the impulse response in the single-axis tilting geometry. We found that angular filtering leads to an overall smoothing of single-axis tomographic reconstructions and to an easier interpretation of reconstructed volumes, particularly in case of low-dose cryo-electron reconstructions, which contain high amounts of noise due to the limited total dose of electrons that can be used for tomogram acquisition before the specimen under observation becomes unacceptably damaged (e.g., Koster and Barcena, 2006).

In this study, we present early results of an analysis of the effect of angular filtering on the resolution of sub-tomogram averages. In sub-tomogram averaging, identical structural motifs appearing in random orientations within one or more reconstructed electron tomographic volumes are semi-automatically located, aligned and averaged in order to produce a 3D map of electron density with a higher signal-to-noise ratio (Ofverstedt et al., 1997; Frangakis et al., 2002; Frangakis and Rath, 2006). This technique is especially helpful in cryo-electron tomography of frozen-hydrated specimens where it greatly simplifies interpretation of subtle biologically significant structures, which appear distorted in reconstructed tomograms due to high amounts of additional noise and the missing wedge artefacts.

Material and Methods

Four single-axis cryo-electron tomographic reconstructions containing repetitive structures were inspected, all of them were reconstructed by the weighted back-projection method in the IMOD reconstruction software for electron tomography (Kremer et al., 1996).

Inspected datasets

Cryo-ET reconstruction of whole cells of *Trypanosoma brucei*

Specimen preparation for electron tomography and acquisition of cryo-EM tomograms was described earlier in Höög et al. (2012). In short, low-dose single-axis tilting series of portions of whole-plunged cells of *T. brucei* were acquired at a Tecnai F30 TEM (FEI, Hillsboro, OR) equipped with a 300 kV FEG, 4K Gatan UltraCam CCD and the Tridiem Gatan Imaging Filter. Eighty-one projections with angular spacing of 1.5° were acquired at the 27,500× magnification within the ± 60° angular range in the zero-loss mode of the energy filter with an energy window of 20 eV at the nominal defocus of -6 μm. The total dose was 90 e-/Å^2. Reconstructions were low-pass filtered with a cutoff of 3 nm and non-linear anisotropic diffusion (NAD) filtered (Frangakis and Hegerl, 2001) also in IMOD, with k = 0.01 and 20 iterations. NAD filtering was performed after angular and low-pass filtering. Fifty-five volumes of 100×100×40 pixels containing the repetitive para-flagellar rod (PFR) structure were located in the flagellum of *T. brucei* and extracted from a single reconstructed stack and subjected to sub-volume averaging. The final pixel size in the sub-volume average corresponded to 0.94 nm.

Cryo-ET reconstructions of axonemes isolated from *Chlamydomonas reinhardtii* cells

Two single-axis tilting reconstructions of axonemes isolated from the flagella of (i) the pseudo wild-type (pwt) of *C. reinhardtii* cells (phenotypically, biochemically, and structurally undistinguishable from wild-type (Rupp and Porter, 2003) and (ii) the 6E6 mutant cells of *C. reinhardtii* (exhibiting reduced motility and structural defects in the flagella (Dymek et al., 2011)) are available as a sample dataset for sub-volume averaging with the PEET package at ftp://bio3d.colorado.edu/pub/PEET/sampleDatasets/Axoneme/. The reconstructions were created by Heuser et al. (2012); preparation of the isolated axonemes for electron tomography is described in Heuser et al. (2012) and Nicastro (2009). In their experiments, tomogram images were obtained with a Tecnai F30 TEM (FEI) at 300 kV accelerating voltage tilted typically from −65 to +65° in 1.5–2.5° angular increments at a magnification of 13,500×, with a final pixel size of 1 nm. The accumulative electron dose was restricted to ~100 e/Å^2 to avoid radiation damage. The reconstruction was not treated by any filter prior to sub-volume averaging. One hundred and fifty-nine and 162 sub-volumes 50×50×50 voxels large containing an axonemal repeat with three radial spokes (Heuser et al., 2012) were extracted from reconstructed stacks of the axonemes of the pseudo wild-type and the 6E6 mutant of *C. reinhardtii*, respectively. The final pixel size in the sub-volume average corresponded to 2 nm.

Cryo-ET reconstructions of Eg5-microtubule complexes

A single-axis tilting reconstruction of microtubules in complex with the Eg5 monomeric motor domain is also available as a sample dataset for sub-volume averaging with the PEET package at ftp://bio3d.colorado.edu/pub/PEET/sampleDatasets/MT/. Specimen preparation and computation of reconstructions are described in Cope et al. (2010). In this experiment, tomogram images were obtained with a Tecnai F20 TEM (FEI) at 200 kV accelerating voltage tilted typically from −60 to +60° in 1.5° angular increments at a magnification of 29,000×, with a final pixel size of 0.9 nm. The accumulative electron dose was restricted to ~100 e/Å^2 to avoid radiation damage. The reconstruction was not treated by any filter prior to sub-volume averaging. Two hundred and forty-one sub-volumes 46×54×46 voxels large containing six helical repeats of the microtubule were extracted from the reconstructed stacks and subjected to sub-volume averaging. After imposing the 15-fold symmetry, the number of averaged subunits increased to 2590. The final pixel size in the sub-volume average corresponded to 0.9 nm.

Angular filtering

Angular and low-pass filtering of raw reconstructed datasets was performed with the BflyTool package for angular filtering (Kovacik et al., 2014); the values of the highest-tilt angles necessary as input parameters for successful angular filtering were measured in Matlab (MathWorks, Natick, MA) individually for each reconstruction. In all cases, the parameters of the angular filter used followed recommendations provided in Kovacik et al. (2014) and had these parameters:

- Profile of both the missing wedge and central stripe ramps: 4th order Butterworth
- Length of the missing-wedge ramp: 65 pixels
- Weight of the missing-wedge ramp at the highest-tilt projection: 0.2
- Central stripe cutoff length: 24 pixels

Sub-volume averaging

Sub-volume averaging was performed with the PEET package (Nicastro et al., 2006) of the IMOD software prior to and after angular filtering of the reconstructed datasets. In order to minimize the missing wedge artefacts and to combine the individual particle data into the final average, the PEET package allows weighted averaging in Fourier space instead of in object space, with each particle contributing to the final averaged volume only with regions lying outside of its tomographic missing wedge. All sub-volume averages in this study were computed with this option. Furthermore, the PEET package also allows randomization of initial orientations of individual particles, which can be used to restrict angular search ranges for particles possessing some kind of symmetry. This option basically increases the chance that the search algorithm finds a local maximum outside of the missing wedge, and therefore further reduces the influence of the missing portion of data in source tomograms. Apart from algorithmic enhancements reducing the effect of the missing projection data, the symmetry of specimens (if present) can be exploited directly, so that only volumes containing individual asymmetric subunits are subjected to averaging, which leads to reduction of both the noise and the missing wedge artefacts in the final averages because they are contributed to by a larger number of asymmetric subunits with varying spatial orientations.

While the PFR and the axoneme sub-volumes do not possess any symmetry that could be directly employed to eliminate the missing-wedge artefacts, the individual αβ-tubulin subunits of the microtubules decorated with the Eg5 monomers are arranged in a 15-fold helix along the axis of the microtubule, with a pitch of 8 nm. Therefore, we used both the randomization of initial orientations and the reduction of the search range in order to estimate the effect of angular filtering on the resolution of symmetric averages.

Resolution of the averaged volumes was estimated by the calcFSC programme of the PEET package at the conservative level of the Fourier shell correlation (FSC) coefficient (Frank, 2006b) of 0.5. The FSC coefficient is calculated in Fourier space after alignment of all extracted sub-volumes. The extracted sub-volumes are then randomly split into two groups of equal size, and the FSC coefficient is computed by comparing their averages in 3D Fourier space (Nicastro et al., 2006).

Results and Discussion

The resolution of averaged particles extracted from original and angularly filtered reconstructions, estimated at the level of 0.5 of the FSC coefficient, is presented in Table 1.

1. Symmetric microtubule-Eg5 complexes

Inspecting the resolution of sub-volume averages computed from the tomogram of highly symmetric microtubules prior to angular filtering (lines 4–6 in Table 1), it is obvious that both randomization of initial orientations and full utilization of symmetry increase the achieved resolution. As expected, it is in particular the full symmetry utilization that advances the resolution, in this case by ~0.56 nm. In contrast to this improvement, sub-volume averages computed from angularly filtered volumes did not significantly alter the resolution of the symmetrized averages. There is only one small improvement of ~0.1 nm in case of the unsymmetrized sub-volume averages.

2. Asymmetric sub-volumes

Averaged sub-volumes with no symmetry (axonemes) or volumes whose symmetry is difficult to exploit (para-

Table 1. Resolution of averaged structural motifs aligned and extracted from 3D reconstructions prior to and after angular filtering, estimated by the Fourier shell correlation (FSC) at level 0.5

	Specimen	Number of averaged sub-volumes	FSC = 0.5 resolution (nm)		Difference (nm)
			unfiltered	filtered	
1	Paraflagellar rod	55	5.65	5.43	-0.22
2	Axoneme pWT	159	5.18	5.13	-0.05
3	Axoneme 6E6	162	5.37	5.13	-0.25
4	Microtubule, no symmetry utilization	241	3.85	3.75	-0.10
5	Microtubule, random axial rotations	241	3.78	3.80	0.02
6	Microtubule, random axial rotations and symmetrization	2590	3.29	3.26	-0.03

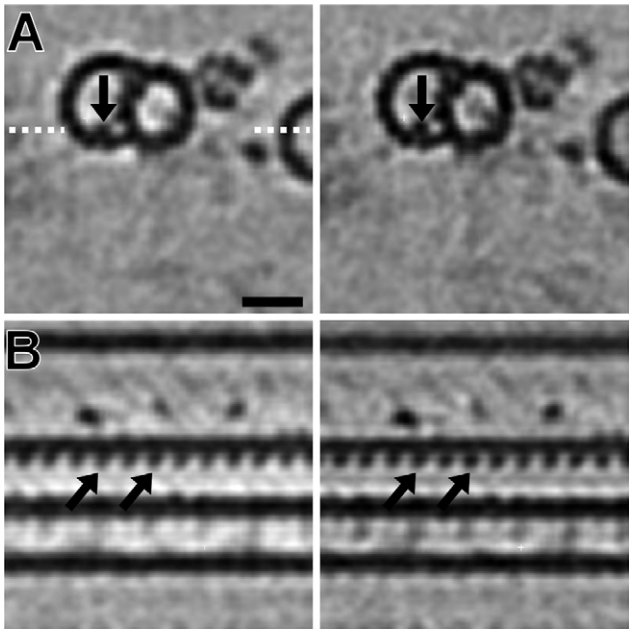

Fig. 1. Two cross-sections through sub-volume averages of an axonemal microtubule doublet of the 6E6 mutant of the *C. reinhardtii* strain. Arrows point at the microtubule inner proteins (Nicastro et al., 2011), which appear better resolved in the sub-volume average computed from angularly filtered reconstructions (right panels) than in the angularly unfiltered counterpart (left panels). The dotted white lines in (**A**) indicate position of cross-sections presented in (**B**), which are perpendicular to cross-section in (A). Scale bar: 20 nm.

flagellar rod) computed from angularly filtered tomograms all have higher resolution than their unfiltered counterparts. While the PFR and 6E6 axoneme averages extracted from angularly filtered tomograms exhibit resolution increased by > 0.2 nm compared to their unfiltered counterparts, the gain is only ~0.05 nm for the pWT axonemes. Figure 1 shows that even the improvement of ~0.2 nm suffices to improve interpretability of the final averages of the 6E6 axonemes. In particular, the individual tubulin subunits and the microtubule inner proteins appear clearly in the average computed from the angularly filtered volume, while they are considerably smeared in the unfiltered sub-volume average.

Conclusions

The acquired results indeed confirm that sub-volume averaging is capable of successful management of the missing-wedge artefacts and other noise occurring in single-axis tilting electron tomographic reconstructions, particularly if orientations of individual particles extracted from the reconstructed stacks are distributed over the full spherical range or if symmetry of the specimen can be used to fill the data-free missing-wedge area in the Fourier space of the averaged volume. In such cases, angular filtering seems to be of little use, as indicated by the achieved resolutions of the sub-volume averages of the Eg5-decorated microtubule repeats. If, however, a limited number of individual particles exhibit a preferential orientation within the reconstructed stacks, which is the case of the 6E6 axonemal and paraflagellar rod sub-volumes, then the reduction of the side-ray artefacts in the reconstructed stacks may increase the resolution of the final sub-volume average. In comparison, while a ~10-fold increase of the number of randomly oriented asymmetric subunits (in the case of Eg5-decorated microtubules) resulted in a resolution increased by ~0.56 nm, angular filtering alone was capable of increasing the resolution by as much as ~0.25 nm (6E6 axonemes) at the same number of averaged sub-volumes.

Acknowledgements

We are very grateful to Johanna L. Höög from the Max Planck Institute of Molecular Cell Biology and Genetics in Dresden for providing us with a dataset of the *T. brucei* reconstruction, John Heumann from the Boulder Laboratory for 3-D Electron Microscopy of Cells, Electron Microscopy of Cells Department of MCD Biology, University of Colorado, Boulder, Colorado, USA, for providing us with the datasets of the microtubule-Eg5 complexes, and Daniela Nicastro from the Brandeis University, Waltham, Massachusetts, USA, for providing us with the axoneme datasets.

References

Carazo, J.-M. (1992) The fidelity of 3D reconstructions from incomplete data and the use of restoration methods. In: *Electron Tomography*, ed. Frank, J., pp. 117-166, Plenum Press, New York.

Cope, J., Gilbert, S., Rayment, I., Mastronarde, D., Hoenger, A. (2010) Cryo-electron tomography of microtubule-kinesin motor complexes. *J. Struct. Biol.* **170**, 257-265.

Dymek, E. E., Heuser, T., Nicastro, D., Smith, E. F. (2011) The CSC is required for complete radial spoke assembly and wild-type ciliary motility. *Mol. Biol. Cell* **22**, 2520-2531.

Frangakis, A. S., Hegerl, R. (2001) Noise reduction in electron tomographic reconstructions using nonlinear anisotropic diffusion. *J. Struct. Biol.* **135**, 239-250.

Frangakis, A. S., Bohm, J., Forster, F., Nickell, S., Nicastro, D., Typke, D., Hegerl, R., Baumeister, W. (2002) Identification of macromolecular complexes in cryoelectron tomograms of phantom cells. *Proc. Natl. Acad. Sci. USA* **99**, 14153-14158.

Frangakis, A. S., Rath, B. K. (2006) Motif search in electron tomography. In: *Electron Tomography*, ed. Frank, J., pp. 401-406, Springer, New York.

Frank, J. (2006a) Introduction: principles of electron tomography. In: *Electron Tomography*, ed. Frank, J., pp. 1-15, Springer, New York.

Frank, J. (2006b) *Three-dimensional Electron Microscopy of Macromolecular Assemblies*. pp. 250-251, Oxford University Press, Oxford.

Heuser, T., Dymek, E. E., Lin, J. F., Smith, E. F., Nicastro, D. (2012) The CSC connects three major axonemal complex-

es involved in dynein regulation. *Mol. Biol. Cell* **23**, 3143-3155.

Höög, J. L., Bouchet-Marquis, C., McIntosh, J. R., Hoenger, A., Gull, K. (2012) Cryo-electron tomography and 3-D analysis of the intact flagellum in Trypanosoma brucei. *J. Struct. Biol.* **178**, 189-198.

Komrska, J. (1983) Fraunhofer-diffraction from sector stars. *Opt. Acta* **30**, 887-925.

Koster, A. J., Barcena, M. (2006) Cryotomography: Low-dose automated tomography of frozen-hydrated specimens. In: *Electron Tomography*, ed. Frank, J., pp. 113-161, Springer, New York.

Kovacik, L., Kerieche, S., Hoog, J. L., Juda, P., Matula, P., Raska, I. (2014) A simple Fourier filter for suppression of the missing wedge ray artefacts in single-axis electron tomographic reconstructions. *J. Struct. Biol.* **186**, 141-152.

Kremer, J. R., Mastronarde, D. N., McIntosh, J. R. (1996) Computer visualization of three-dimensional image data using IMOD. *J. Struct. Biol.* **116**, 71-76.

Nicastro, D., Schwartz, C., Pierson, J., Gaudette, R., Porter, M. E., McIntosh, J. R. (2006) The molecular architecture of axonemes revealed by cryoelectron tomography. S*cience* **313**, 944-948.

Nicastro, D. (2009) Cryo-electron microscope tomography to study axonemal organization. *Methods Cell. Biol.* **91**, 1-39.

Nicastro, D., Fu, X. F., Heuser, T., Tso, A., Porter, M. E., Linck, R. W. (2011) Cryo-electron tomography reveals conserved features of doublet microtubules in flagella. *Proc. Natl. Acad. Sci. USA* **108**, E845-E853.

Ofverstedt, L. G., Zhang, K., Isaksson, L. A., Bricogne, G., Skoglund, U. (1997) Automated correlation and averaging of three-dimensional reconstructions obtained by electron tomography. *J. Struct. Biol.* **120**, 329-342.

Penczek, P. A., Frank, J. (2006) Resolution in electron tomography. In: *Electron Tomography*, ed. Frank, J., pp. 307-330, Springer, New York.

Rupp, G., Porter, M. E. (2003) A subunit of the dynein regulatory complex in Chlamydomonas is a homologue of a growth arrest-specific gene product. *J. Cell. Biol.* **162**, 47-57.